The Relative Roles of Sulfate Aerosols and Greenhouse Gases in Climate Forcing

J. T. Kiehl and B. P. Briegleb

Calculations of the effects of both natural and anthropogenic tropospheric sulfate aerosols indicate that the aerosol climate forcing is sufficiently large in a number of regions of the Northern Hemisphere to reduce significantly the positive forcing from increased greenhouse gases. Summer sulfate aerosol forcing in the Northern Hemisphere completely offsets the greenhouse forcing over the eastern United States and central Europe. Anthropogenic sulfate aerosols contribute a globally averaged annual forcing of −0.3 watt per square meter as compared with +2.1 watts per square meter for greenhouse gases. Sources of the difference in magnitude with the previous estimate of Charlson *et al.* are discussed.

Natural and anthropogenic sulfate aerosols play an important climatic role in that they reflect solar radiation back to space (*1*). The reflection of solar radiation back to space by anthropogenic sulfate, called the direct effect, has been estimated to have an annual global mean radiative forcing (*2*) of ~ -1 W m^{-2}. The direct radiative effect is approximately one-half of the forcing, 2.0 to 2.5 W m^{-2}, estimated to have occurred as a result of increases in the concentrations of trace gases since preindustrial times (1750 to 1880) (*1*, *3*). In addition, these aerosols may have an indirect effect on cloud albedo of up to ~ -1 W m^{-2} (*1*). Taken together, the estimated combined direct and indirect effects of sulfate aerosols could cancel virtually all the greenhouse forcing. In this article we address only the direct effect of sulfate aerosols because recent results indicate that the indirect effect has been overestimated (*4*).

Understanding the climatic effects of sulfate aerosols requires a comprehensive approach that includes consideration of both chemical and radiative processes and their spatial distribution. Observations (*5*) and calculations (*6*) before the past 2 years did not directly link the chemical processes that determine the sulfate properties with the important radiative properties that directly determine the aerosol climate forcing. In the past 2 years, significant progress has been made in both of these areas. In particular, important components required for the calculation of the direct effect of aerosol include its amount and spatial distribution. Such calculations have only recently become available (*7*).

In this article we estimate the direct radiative effect of sulfate aerosols and discuss differences from earlier estimates [notably that of Charlson *et al.* (*1*, *2*)]. We also provide a regional comparison of the relative forcing from greenhouse gases and sulfate aerosols.

The authors are with the National Center for Atmospheric Research, Post Office Box 3000, Boulder, CO 80307.

Model Calculations

Earlier regionally specific direct forcing estimates (*2*) were derived from a simple two-layer radiation model. In this model, the measure of the efficiency of visible radiation scattered back to space (backscatter fraction) and the efficiency of scattered visible radiation in the atmosphere (extinction optical depth) was obtained from field observations. The data for these two important aerosol optical properties were based on separate sets of observations. The earlier estimate also used spatially averaged solar insolation, surface properties, and relative humidity (RH).

To account accurately for spatially dependent effects, we used a three-dimensional (3D) diagnostic model to calculate the radiative forcing resulting from a number of greenhouse gases and the sulfate aerosols. The horizontal resolution of the model was 2.8° by 2.8° (roughly 300 km), and there were 18 vertical levels. The model used monthly mean 1989 analyzed temperature and moisture fields from the European Centre for Medium Range Weather Forecasting (ECMWF) (*8*). Vertical distributions of clouds are not readily available, so we obtained cloud amounts from a general circulation model simulation of the National Center for Atmospheric Research (NCAR) Community Climate Model (CCM2). Cloud cover was specified for each grid point and diagnostic model level. The cloud cover in each layer has been renormalized such that the total globally averaged cloud cover agreed with observations (*9*). This normalization ensured a cloud amount identical to that of Charlson *et al.* (*2*). The liquid water path and effective radius of cloud droplets were also obtained from CCM2. Calculated shortwave flux accounts for the diurnal cycle of solar radiation. All calculations were performed for each month of the year, and then results were averaged over the annual cycle.

The model requires calculations of both the shortwave and the longwave fluxes, both of which require several assumptions. The shortwave radiative flux was obtained from a δ-Eddington model (*10*) with 18 spectral intervals (0.2 to 5 μm). The optical properties of clouds were specified for each of the 18 spectral intervals; the optical properties for the sulfate aerosols are discussed below.

The longwave radiation model (*11*) accounted for the radiative effects of H_2O, CO_2, and O_3 as well as the effects of CH_4, N_2O, CFC-11, and CFC-12 (CFC, chlorofluorocarbon). The changes in total radiative flux caused by increases in the trace gases as predicted by the model agree to within 0.2 W m^{-2} with more detailed calculations. Cloud emissivities depend on the specified liquid water distribution of the cloud. The longwave effects of the sulfate aerosol were not considered because we assumed that the aerosol layer is confined to the lowest ≈1 km of the atmosphere. Thus, there was little temperature difference between the aerosol layer and the surface temperature and, hence, little greenhouse effect.

Direct Effect of the Sulfate Aerosols

The direct climate forcing of the sulfate aerosol is a result of increased reflection of solar radiation back to space. To calculate this change in net incoming solar radiation, we needed to specify the radiative properties of the aerosol and the amount and spatial distribution of sulfate in the atmosphere, that is, the sulfate burden. The radiative properties consisted of three factors: (i) the extinction per unit mass, the so-called specific extinction (*12*), Ψ_e; (ii) the single scattering albedo, ω_0, which defines the absorbing efficiency of the particles; and (iii) the asymmetry parameter, g, which is a measure of the amount of radiation scattered toward Earth's surface relative to that scattered back to space. Values of g range from −1 (complete backward

scattering) to +1 (complete forward scattering).

These optical properties can be evaluated from standard Mie theory once the index of refraction (which depends on the chemical composition) and size distribution of the aerosol have been determined. We assumed that the size distribution for the aerosols was log-normal (*13*). The geometric mean radius by number $\bar{r}_n$ was specified as equal to 0.05 μm; the geometric standard deviation σ_g was 2.0. These values imply that the geometric mean diameter by volume (DGV) is 0.42 μm, which falls within the range of observational data (0.37 to 0.44 μm) for sulfate aerosols (*13*, *14*). The index of refraction for the sulfate aerosol was based on data in (*15*). These data give the index of refraction for a range of wavelengths. We assumed that the aerosol contained 75% H_2SO_4 and 25% H_2O (*16*).

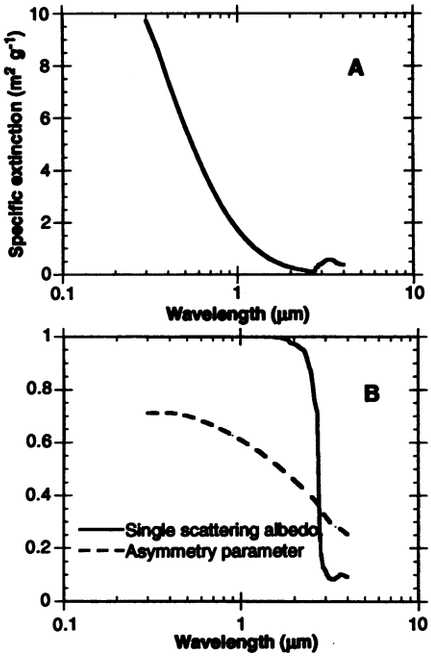

Fig. 1. (**A**) Dry air sulfate specific extinction (in square meters per gram) as a function of wavelength (in micrometers). (**B**) Single scattering albedo, ω_0, and asymmetry parameter, *g*, as a function of wavelength.

The aerosol specific extinction $\Psi_e(\lambda)$ for a given wavelength λ is obtained from

$$\Psi_e(\lambda) = \frac{3}{4\rho_s} \frac{\int Q_e(\lambda,r) r^2 n(r) dr}{\chi_{SO_4} \int r^3 n(r) dr} f(\mathrm{RH})$$

where integration is over the particle radius *r*; $Q_e(\lambda,r)$ is the Mie extinction efficiency parameter; $n(r)$ is the log-normal size distribution; and χ_{SO_4} is the fraction of fine-particle mass that is sulfate. Observations suggest that this fraction is between 55 and 65% (*17*); we therefore used 60%. The sulfate dry particle density ρ_s is assumed to be 1.7 g cm^{-3} (*13*).

The parameter f(RH) accounts for the dependence of particle size on RH; RH is defined as the boundary layer RH. Increased RH results in larger particles, which scatter more radiation. The form of this function was obtained from a fit to observations of the ratio of light scattering at a relative humidity RH to the scattering at RH = 30% (*18*). We evaluated f(RH) from the ECMWF temperature and specific humidity data at each grid point. The regional variation of f(RH) is quite large (roughly a factor of 3) because of the regional variation in RH. The remaining optical parameters, ω_0 and *g*, are determined from the size distribution $n(r)$ (*19*). These optical properties should also be scaled by a relative humidity factor (*20*), but observational data are lacking on the exact functional dependence. We therefore did not explicitly include this relation.

The calculated sulfate specific extinction (Fig. 1A) exhibits a strong spectral dependence. In the visible region, Ψ_e decreases as $\approx\lambda^{-1.1}$; the exponent (the angstrom coefficient) of 1.1 agrees well with observations. The variation of ω_0 (Fig. 1B) indicates that the sulfate aerosols are nonabsorbing in the visible spectral region. The asymmetry parameter decreases monotonically in the near infrared region (λ ≈ 1 μm).

The final quantities needed to calculate the direct effect of the aerosol are the amount and spatial distribution of the sulfate aerosol. We used monthly mean sulfate abundances from (*2*, *7*). Sulfate distributions were obtained from a 3D chemical-transport model (*7*). We assumed that the total sulfate burden is well mixed in the boundary layer [that is, approximately the lowest 1 km of the atmosphere (*21*)].

The calculated annual mean change in absorbed solar radiation due to anthropogenic and total (natural + anthropogenic) sulfate aerosols, respectively, shows a pronounced spatial pattern (Fig. 2). This pattern agrees well with that determined by Charlson *et al.* (*2*). However, the magnitude is generally less by a factor of 2, as seen in the globally averaged results (Table 1). The largest anthropogenic forcing is located over the eastern United States, southeastern Europe, and eastern China. These large forcing values are a direct result of the large sulfate burdens for these industrial regions. There is also a large forcing in Africa related to a local maximum in sulfate in this region (*7*). In general, the anthropogenic forcing dominates the natural forcing, except in oceanic regions.

To identify the sources of the difference in magnitude with the results of Charlson *et al.* (*2*), we carried out forcing calculations using both our method and their method. The analysis revealed that roughly half of the difference is due to the fact that Charl-

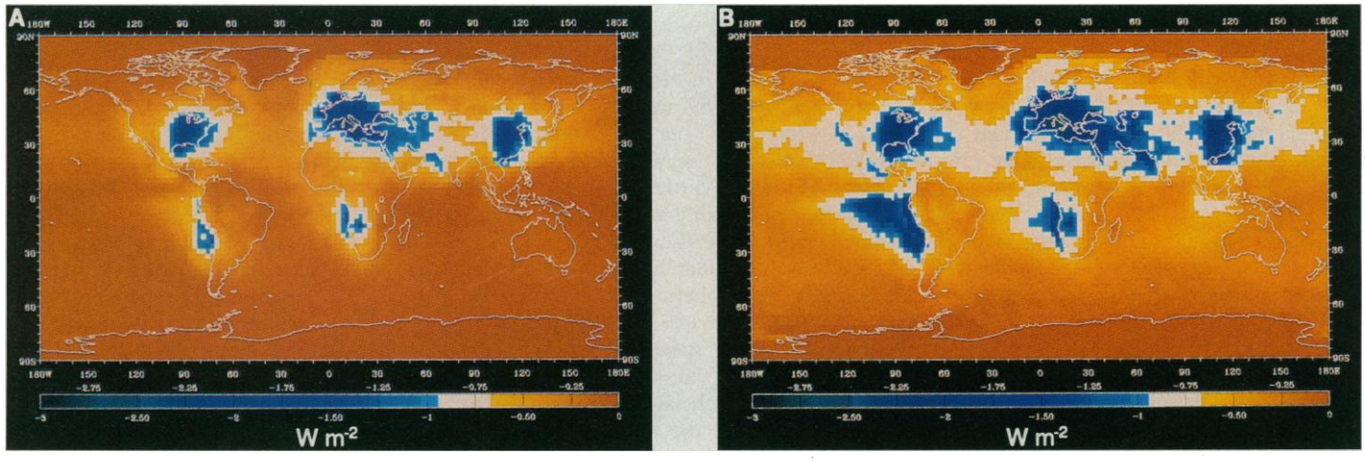

Fig. 2. Annual mean direct forcing (in watts per square meter) resulting from (**A**) anthropogenic sulfate aerosols (global = −0.28 W m^{-2}) and (**B**) anthropogenic plus natural sulfate aerosols (global = −0.54 W m^{-2}).

son *et al.* (*1*, *2*) assumed a constant specific extinction (Ψ_e = 5 m^2 g^{-1} for low RH conditions). Figure 1A indicates that this value is valid only for visible wavelengths. Although Ψ_e is larger for wavelengths of less than 0.55 μm, there is little near-surface solar radiation available at these wavelengths. For wavelengths greater than 0.55 μm, Ψ_e decreases rapidly and hence leads to smaller aerosol forcing. A second source of difference results from differences in the asymmetry parameter. Charlson *et al.* (*2*) used a *g* value of 0.52 (*22*), whereas our visible value was 0.69. If we had used a *g* value of 0.52, our direct forcing would have increased by 25%, which is in better agreement with their results. However, the value of *g* cannot arbitrarily be decreased without affecting Ψ_e. Calculations show that, if *g* is reduced by 25%, Ψ_e decreases by more than a factor of 2. These changes compensate one another such that the total forcing changes by only a few percent. Our calculated optical properties are self consistent because they are determined by an assumed size distribution and chemical composition. Present observations are insufficient to determine why calculated and observed *g* and Ψ_e values disagree.

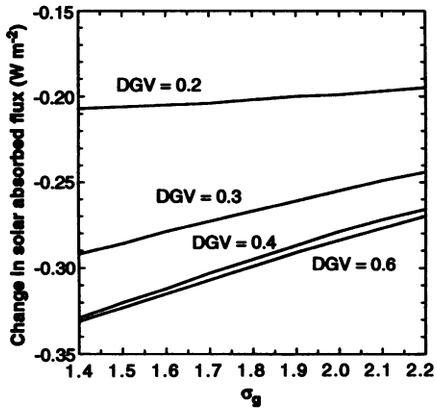

Fig. 3. Globally averaged direct sulfate forcing (in watts per square meter) as a function of the width of the particle size distribution, σ_g, for four geometric mean diameters (DGV = 0.2, 0.3, 0.4, and 0.6 μm).

The dependence of the forcing on these optical properties is also dependent on assumptions about the chemicophysical nature of the sulfate aerosol. Chemical properties determine the refractive index of the aerosol, which can alter the optical properties. For example, with surface sources of ammonia (NH_3), the dominant chemical form of the sulfate aerosol may be ammonium sulfate [$(NH_4)_2SO_4$], not acidic sulfate (H_2SO_4 or NH_4HSO_4) (*17*, *23*). The real part of the refractive index of ammonium sulfate is 6% larger than that of H_2SO_4 (*24*). This increase in refractive index leads to a 25% increase in Ψ_e and a 6% decrease in *g*. However, the *f*(RH) of ammonium sulfate, unlike that of acidic sulfate, is equal to 1 for RHs below 80% (*25*). Values of RH over land from the ECMWF data are generally less than 80% (even in summer). Thus, although *f*(RH) is equal to 1.7 to 1.8 over land for H_2SO_4, it is equal to 1 for ammonium sulfate. This difference in *f*(RH) leads to an ammonium sulfate forcing that is only 5% larger than the H_2SO_4 value.

Chemicophysical processes can also affect the size distribution of the sulfate particles. To indicate the dependence of the physical characteristics of the aerosol on direct forcing, we calculated the globally averaged direct radiative forcing as a function of the width of the particle size distribution (Fig. 3). The results indicate that, for a 25% decrease (increase) in the width of the size distribution, the direct forcing increases (decreases) by roughly 14%. We assumed that the particles are represented by a single log-normal size distribution, but accurate representation of aerosol distributions typically requires two or more log-normal distributions. The addition of differing size distributions can also affect the optical properties (*26*).

These sensitivity studies indicate that our direct sulfate forcing could be altered by ±10% as a result of variations in size or chemical composition. The actual magnitude and spatial distribution of the sulfate forcing depend on the spatial distribution of a number of chemical and physical processes. To define better the direct forcing due to sulfate aerosols, more comprehensive and simultaneous observational data are needed on the chemical, physical, and radiative properties of the aerosol. These data are needed for a range of different geographic locations because the sulfate characteristics are no doubt linked to the chemical environment (for example, NH_3 sources).

Table 1. Area-averaged direct sulfate forcing (in watts per square meter) due to sulfate aerosols. Values in parentheses are the estimates from (*2*).

Location	Natural	Anthropogenic	Total
Northern Hemisphere	−0.29 (−0.50)	−0.43 (−1.07)	−0.72 (−1.57)
Southern Hemisphere	−0.25 (−0.35)	−0.13 (−0.11)	−0.38 (−0.46)
Global	−0.26 (−0.42)	−0.28 (−0.60)	−0.54 (−1.02)

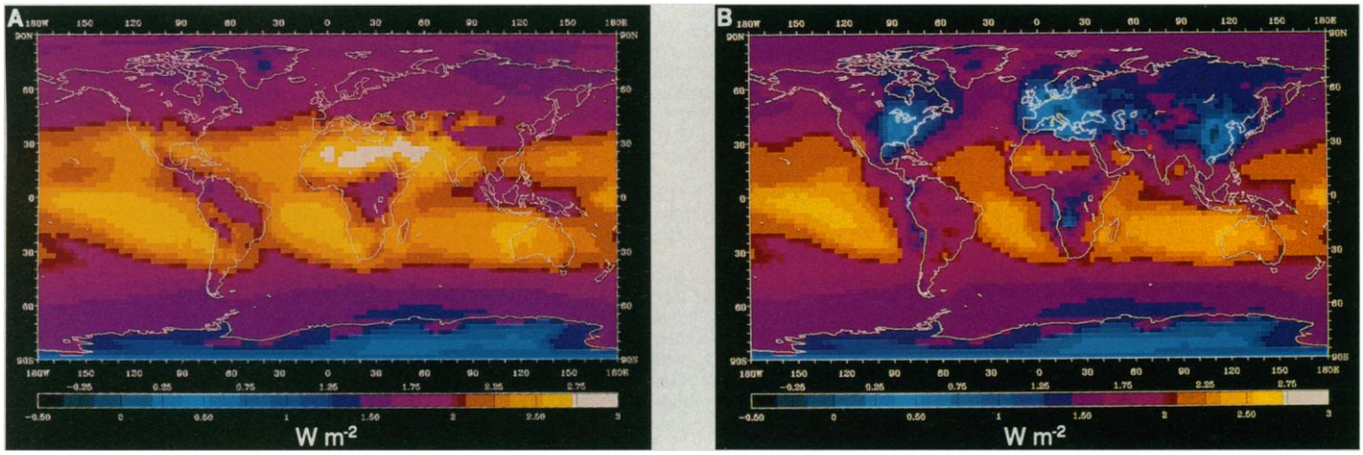

Fig. 4. (**A**) Annual averaged greenhouse forcing (in watts per square meter) from increases in CO_2, CH_4, N_2O, CFC-11, and CFC-12 from preindustrial time to the present (global = 2.1 W m^{-2}). (**B**) Annual averaged greenhouse forcing plus anthropogenic sulfate aerosol forcing (in watts per square meter) (global = 1.8 W m^{-2}).

Relative Role of Direct Sulfate Forcing

Despite our smaller forcing values compared with those of Charlson *et al.* and also the uncertainties in the direct sulfate forcing due to uncertainties in the chemical and physical characteristics of the aerosol, the regional changes in the absorbed solar radiation (Fig. 2) are quite significant compared with the trace gas greenhouse effect. To understand these changes, we compare this negative forcing of the climate system with the positive forcing caused by increases in greenhouse gases.

Most estimates of the climate forcing resulting from increased greenhouse gases have been given for either global mean averages or perhaps zonal averages (*27–29*). Although these calculations are useful for estimating the potential climatic effects for increases in these gases (CO_2, CH_4, N_2O, or halocarbons), they do not indicate the magnitude of the regional variations of this forcing. We thus calculated the spatial distribution of the change in the net longwave flux at the tropopause level (*3*) for the trace gas increases from preindustrial to present gas concentrations. These values are those defined by the Intergovernmental Panel on Climate Change (IPCC) (*30*). Preindustrial values are as follows: CO_2, 280 parts per million by volume (ppmv); CH_4, 0.8 ppmv; N_2O, 0.288 ppmv; CFC-11, 0 ppbv; and CFC-12, 0 ppbv. Present values are as follows: CO_2, 353 ppmv; CH_4, 1.72 ppmv; N_2O, 0.310 ppmv; CFC-11, 0.28 ppbv; and CFC-12, 0.484 ppbv. We did not include a lower stratospheric O_3 reduction in our greenhouse forcing estimates (*29*), nor did we include forcing from other CFCs.

The annual averaged change in greenhouse forcing (Fig. 4A) resulting from an increase in trace gas levels from the preindustrial time to the present varies with location by a factor of 5, with the largest forcings occurring in warm dry regions. In these regions the spectral overlap of water vapor with the greenhouse gases is small, and the difference between the surface temperature and the atmospheric temperature is greater, which enhances the greenhouse effect. Tropical regions where the degree of cirrus cloud cover is large are regions of small forcing because of the shielding effect of these high clouds. The globally averaged change in forcing from preindustrial times is 2.1 W m^{-2}, similar to previous estimates (*3*).

The change in forcing for the preindustrial period to the present (Fig. 4B) is the combined effect of greenhouse (Fig. 4A) and anthropogenic sulfate aerosol forcing (Fig. 2A). In the Northern Hemisphere there are regions over land where the aerosol effect is actually larger than the greenhouse effect. Thus, a net negative forcing occurs in very local regions of the eastern part of the United States, south central Europe, and eastern China. In Northern Hemisphere summer, because of greater solar insolation, the region of negative forcing extends over the eastern half of the United States. The region of negative forcing in eastern Europe is also larger in summer.

Relevance to Other Aerosol Studies

A number of these conclusions can be generalized to the problem of the climatic effects of other aerosols. In particular, in recent estimates of the climate forcing due to smoke (*31*), aerosols use the same simple radiative model of Charlson *et al.* (*2*), where the aerosol specific extinction is assumed to be independent of wavelength. Most aerosols exhibit a decrease in extinction with wavelength. Thus, the radiative effects of smoke have probably been overestimated. A detailed analysis such as the present one for sulfate aerosols would reveal to what extent these effects have been overestimated. The remaining aerosols of importance are those composed of elemental carbon. Estimates of the spatial effects of these aerosols on the climate system are urgently needed.

REFERENCES AND NOTES

1. R. J. Charlson *et al.*, *Science* **255**, 423 (1992).
2. R. J. Charlson, J. Langner, H. Rodhe, C. B. Leovy, S. G. Warren, *Tellus* **43AB**, 152 (1991).
3. T. M. L. Wigley and S. C. B. Raper [*Nature* **357**, 293 (1992)] indicated a range in preindustrial to 1990 greenhouse forcing of about 2.15 to 2.45 W m^{-2}. K. P. Shine *et al.* [in *Climate Change: The IPCC Scientific Assessment*, J. T. Houghton *et al.*, Eds. (Cambridge Univ. Press, Cambridge, 1990), pp. 41–68] calculated a greenhouse forcing from preindustrial time to 1990 of 2.45 W m^{-2} with a stated uncertainty of at least ±10%.
4. J. Langner, H. Rodhe, P. J. Crutzen, P. Zimmermann, *Nature* **359**, 712 (1992).
5. R. J. Ball and G. D. Robinson, *J. Appl. Meteorol.* **21**, 171 (1982).
6. J. A. Coakley, R. D. Cess, F. B. Yurevich, *J. Atmos. Sci.* **40**, 116 (1983).
7. J. Langner and H. Rodhe, *J. Atmos. Chem.* **13**, 225 (1991).
8. Monthly mean global data for the 3D diagnostic model are taken from the following sources: temperature and specific humidity profiles, K. E. Trenberth and J. G. Olson, *Tech. Note NCAR/TN-300+STR* (1988); O_3 profiles, D. L. Williamson, J. T. Kiehl, V. Ramanathan, R. E. Dickinson, J. J. Hack, *Tech. Note NCAR/TN-285+STR* (1987); sea-surface temperature data, R. W. Reynolds, *J. Clim.* **1**, 75 (1988); land surface temperatures, D. R. Legates and C. J. Willmott, *Theor. Appl. Climatol.* **41**, 11 (1989).
9. S. G. Warren, C. J. Hahn, J. London, R. M. Chervin, R. L. Jenne, *NCAR Tech. Note TN-273+STR* (1986).
10. B. P. Briegleb, *J. Geophys. Res.* **97**, 7603 (1992).
11. ———, *ibid.*, p. 11475.
12. V. Ramaswamy and J. T. Kiehl, *ibid.* **90**, 5597 (1985).
13. K. T. Whitby, *Atmos. Environ.* **12**, 135 (1978).
14. ——— and G. M. Sverdrup, in *The Character and Origins of Smog Aerosols*, G. M. Hidy *et al.*, Eds. (Wiley, New York, 1980), pp. 477–517.
15. K. F. Palmer and D. Williams, *Appl. Opt.* **14**, 208 (1975).
16. The index of refraction varies by less than 3% for mixtures ranging from 50 to 85% H_2SO_4 and from 50 to 15% H_2O.
17. R. E. Weiss, T. V. Larson, A. P. Waggoner, *Environ. Sci. Technol.* **16**, 525 (1982).
18. R. J. Charlson, D. S. Covert, T. V. Larson, in *Hygroscopic Aerosols*, L. H. Ruhnke and A. Deepak, Eds. (Deepak, Hampton, VA, 1984), pp. 35–44.
19. S. Twomey, *Atmospheric Aerosols* (Elsevier, Oxford, 1977).
20. G. Hänel, *Adv. Geophys.* **19**, 73 (1976).
21. Sensitivity studies based on the use of a single-column radiation model indicate that, if half of the aerosol is distributed above the lowest 1 km, the direct forcing can decrease by up to 10%. Although placing part of the aerosol above the cloud layers should increase the direct forcing, the RH above the lowest kilometer in the atmosphere is lower, so that the f(RH) in Ψ_e decreases. This decrease in f(RH) more than compensates for the aerosol loading above cloud top.
22. Charlson *et al.* (*2*) used backscatter fraction, b, rather than g. There is a one-to-one correspondence between b and g [W. J. Wiscombe and G. W. Grams, *J. Atmos. Sci.* **33**, 2440 (1976)], and hence either measure of the amount of radiation scattered in the forward or backward direction can be used for the direct aerosol forcing problem. A value of $g = 0.52$ corresponds to $b = 0.15$, whereas $g = 0.69$ is equivalent to $b = 0.1$. Our value for g was obtained from Mie theory calculations; the g value used in (*2*) was based on observational data from selected sites. Given the importance of g (or b) to the direct forcing problem, more observational data are needed for a diverse range of locations and times of year.
23. R. E. Weiss, A. P. Waggoner, R. J. Charlson, N. C. Ahlquist, *Science* **195**, 979 (1977).
24. O. B. Toon, J. B. Pollack, B. N. Khare, *J. Geophys. Res.* **81**, 5733 (1976).
25. K. T. Whitby, in *Hygroscopic Aerosols*, L. H. Ruhnke and A. Deepak, Eds. (Deepak, Hampton, VA, 1984), pp. 45–63.
26. C. W. Lewis, *Atmos. Environ.* **15**, 2639 (1981).
27. See Wigley and Raper [in (*3*)].
28. T. M. L. Wigley, *Nature* **349**, 503 (1991).
29. V. Ramaswamy, M. D. Schwarzkopf, K. P. Shine, *ibid.* **355**, 810 (1992).
30. R. T. Watson *et al.*, in *Climate Change: The IPCC Scientific Assessment*, J. T. Houghton *et al.*, Eds. (Cambridge Univ. Press, Cambridge, 1990), pp. 1–40.
31. J. E. Penner, R. E. Dickinson, C. A. O'Neill, *Science* **256**, 1432 (1992).

32. This work has benefited greatly from many conversations with R. Charlson and comments by T. M. L. Wigley. We also thank J. Langner for supplying the sulfate data. This work was supported in part by Earth Observing System project W-17,661. The National Center for Atmospheric Research is sponsored by the National Science Foundation.